NMR IN BIOMEDICINE
NMR Biomed. 2006; **19**: 288–299
Published online in Wiley InterScience (www.interscience.wiley.com). DOI:10.1002/nbm.1042

Encoding and Reconstruction in Parallel MRI

Klaas P. Pruessmann*

Institute for Biomedical Engineering, University and ETH Zurich, Zurich, Switzerland

Received 15 February 2005; Accepted 14 March 2006

ABSTRACT: The advent of parallel MRI over recent years has prompted a variety of concepts and techniques for performing parallel imaging. A main distinguishing feature among these is the specific way of posing and solving the problem of image reconstruction from undersampled multiple-coil data. The clearest distinction in this respect is that between *k*-space and image-domain methods. The present paper reviews the basic reconstruction approaches, aiming to emphasize common principles along with actual differences. To this end the treatment starts with an elaboration of the encoding mechanisms and sampling strategies that define the reconstruction task. Based on these considerations a formal framework is developed that permits the various methods to be viewed as different solutions of one common problem. Besides the distinction between *k*-space and image-domain approaches, special attention is given to the implications of general vs lattice sampling patterns. The paper closes with remarks concerning noise propagation and control in parallel imaging and an outlook upon key issues to be addressed in the future. Copyright © 2006 John Wiley & Sons, Ltd.

KEYWORDS: parallel MRI; *k*-space; image domain; SMASH; SENSE; GRAPPA; electrodynamics; spatial degrees of freedom

INTRODUCTION

Parallel MRI relies on the simultaneous detection of magnetic resonance with multiple receiver coils surrounding the object under examination. In this fashion multiple signals of distinct information content are obtained at one time, marking the key advantage of the parallel approach over standard Fourier MRI. Different coil elements yield different information because each exhibits an individual spatial reception characteristic, corresponding to a distinct spatial encoding effect. The latter can be used to complement and hence reduce conventional gradient encoding, leading to faster imaging and numerous derived benefits.

The basic idea of parallel MRI dates back to the late 1980s when first concepts were proposed by Carlson (1), Hutchinson *et al.*(2) and Kelton *et al.*(3), followed by further contributions by Kwiat *et al.*(4), Carlson *et al.*(5) and Ra *et al.*(6) in the early 1990s. However, only in the late 1990s was parallel detection first successfully used for actually accelerating an MRI procedure. This second era of parallel MRI development was triggered by the introduction of the SMASH technique (Simultaneous acquisition of spatial harmonics) (7), followed by the SENSE approach (sensitivity encoding) (8,9). Since then the family of parallel imaging methods has quickly grown, now including a range of further variants such as PILS (parallel imaging with localized sensitivities) (10), SPACERIP (sensitivity profiles from an array of coils for encoding and reconstruction in parallel) (11), generalized SMASH (12), GRAPPA (generalized autocalibrating partially parallel acquisitions) (13), and PARS (parallel imaging with augmented radius in *k*-space) (14).

The increasing use of parallel detection in MRI (15,16) has far-reaching consequences with respect to radiofrequency instrumentation, data acquisition, data processing and image properties. Many of these implications are quite similar for the various parallel imaging techniques. One distinguishing feature, however, is the specific way of posing and solving the problem of image reconstruction from multiple-coil data. The existing methods are often categorized into *k*-space and image-domain approaches, based on the data representation used for performing the essential reconstruction steps. These two views lead to quite different formalisms and procedures, marking one reason for the present variety of coexistent techniques. Besides permitting efficient reconstruction, the two views also offer useful intuition for conceptual considerations, coil array design and identifying sampling strategies. However, the focus on either *k*-space or image-domain thinking is also problematic. It makes it more

**Correspondence to:* K. P. Pruessmann, Institute for Biomedical Engineering, ETH Zurich, Gloriastrasse 35, CH-8092 Zurich, Switzerland.
E-mail: pruessmann@biomed.ee.ethz.ch

Abbreviations used:: CG, conjugate gradients; DFT, discrete Fourier transform; FOV, field of view; GRAPPA, generalized autocalibrating partially parallel acquisitions (13); PARS, parallel imaging with augmented radius in *k*-space (14); PILS, parallel imaging with localized sensitivities (10); RF, radiofrequency; SENSE, sensitivity encoding (8); SMASH, simultaneous acquisition of spatial harmonics (7); SNR, signal-to-noise ratio; SPACERIP, sensitivity profiles from an array of coils for encoding and reconstruction in parallel (11); SRF, spatial response function.

difficult to pin down differences between algorithms, e.g. in terms of reconstruction fidelity and noise behavior. Perhaps it also tends to overrate conceptual differences, sometimes obscuring that the two domains are only alternative perspectives of a single reconstruction task.

The purpose of the present paper is to review the basic approaches to parallel imaging reconstruction in light of the preceding remarks. Emphasizing distinguishing features is one of its goals. However it is also an attempt to establish a framework that permits the various methods to be viewed as different solutions of one common problem. To this end, the paper focuses on conceptual considerations and generic aspects, including the encoding mechanisms and sampling strategies that define the reconstruction task. Describing each of the current parallel MRI techniques in detail is beyond the scope of this contribution. Rather, for actual algorithms and implementation specifics the reader is referred to the literature.

SPATIAL ENCODING

In standard Fourier MRI the spatial resolution within an image plane (or three-dimensional volume) relies exclusively on gradient fields, which impose plane-wave modulations on the transverse magnetization $M(\boldsymbol{r})$. Precessing in the main field B_0 and the superimposed gradient fields, the magnetization generates radiofrequency (RF) electromagnetic fields, which are detected with one or multiple receiver coils. Neglecting constant factors, a data sample taken with a homogeneously sensitive coil is given by:

$$d_\kappa = \int M(\boldsymbol{r}) e^{j\boldsymbol{k}_\kappa \boldsymbol{r}} \mathrm{d}\boldsymbol{r} \qquad (1)$$

where j denotes the imaginary unit and $\boldsymbol{k}_\kappa$ is the wave vector describing the κth plane-wave encoding. Figure 1 shows an example of one such plane wave, along with its Fourier transform. The latter is a single Dirac peak at $\boldsymbol{k}_\kappa$, reflecting the fact that the encoding operation is equivalent to sampling the Fourier transform of $M(\boldsymbol{r})$ at this position.

The gradient fields directly manipulate the magnetization to be depicted; hence each plane-wave encoding corresponds to a certain magnetization state. As a consequence only one such encoding can be performed at a time, resulting in the long scan durations that are notorious for MRI.

This situation is still essentially the same in traditional phased-array imaging, as described by Roemer *et al.*(17). There a signal sample taken with the γth coil element is given by

$$d_{\gamma,\kappa} = \int M(\boldsymbol{r}) s_\gamma(\boldsymbol{r}) e^{j\boldsymbol{k}_\kappa \boldsymbol{r}} \mathrm{d}\boldsymbol{r} \qquad (2)$$

where $s_\gamma(\boldsymbol{r})$ denotes the coil's complex-valued, spatially varying sensitivity. With full Fourier encoding and standard Fourier reconstruction each coil yields an individual image weighted by the coil sensitivity. The

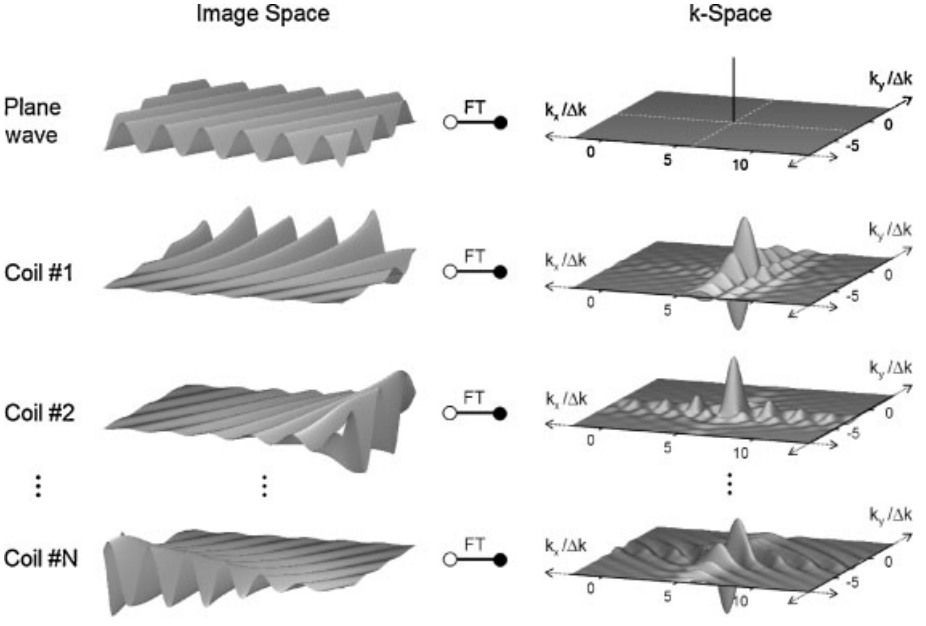

Figure 1. Encoding functions. Top row: example of a plane-wave encoding function as created by gradient fields in standard Fourier MRI ($k_x = 6 \times 2\pi/\mathrm{FOV}$, $k_y = -3 \times 2\pi/\mathrm{FOV}$). Its *k*-space representation is a single Dirac peak at (k_x, k_y). Other rows: hybrid encoding functions, resulting from the same plane wave multiplied with different coil sensitivities. In *k*-space each hybrid encoding function has a distinct shape, which is equal to the Fourier transform of the respective coil sensitivity, shifted by (k_x, k_y). Note that the encoding functions are complex-valued, the plots showing only the real part

essential algorithms for combining such single-coil images were described by Roemer *et al.* in their original work (17). Root-sum-of-squares combination yields a magnitude image with near-optimal signal-to-noise ratio (SNR). A complex image with optimal SNR can be obtained with a matched-filter combination, incorporating the coil sensitivities $\boldsymbol{s}_\gamma(\boldsymbol{r})$ and the noise covariance (or resistance) matrix of the coil array.

In a sense, the transition from this more traditional paradigm to actual parallel MRI hinges on a mere shift of viewpoint. In single-coil reconstruction, $\boldsymbol{s}_\gamma(\boldsymbol{r})$ in eqn. (2) is effectively treated as a modulation of $M(\boldsymbol{r})$, hence causing a modulation of the resulting image. As opposed to that, in parallel MRI $\boldsymbol{s}_\gamma(\boldsymbol{r})$ is considered a modulation of the plane-wave encoding function, leading to the hybrid encoding basis:

$$\mathrm{enc}_{\gamma,\kappa}(\boldsymbol{r}) = s_\gamma(\boldsymbol{r}) e^{j\boldsymbol{k}_\kappa \boldsymbol{r}} \qquad (3)$$

and the encoding equation

$$d_{\gamma,\kappa} = \int M(\boldsymbol{r})\, \mathrm{enc}_{\gamma,\kappa}(\boldsymbol{r})\, \mathrm{d}\boldsymbol{r} \qquad (4)$$

This shift of viewpoint has far-reaching consequences. Figure 1 illustrates that the hybrid encoding functions are no longer pure plane waves but plane waves multiplied by coil sensitivity. Accordingly, in their equivalent *k*-space representation they are no longer Dirac peaks but now have distinct shapes and a significant extent. Mathematically speaking, this is the result of a convolution with the Fourier transform of the respective coil sensitivity function. Hence the hybrid encoding functions of a given coil are all copies of this Fourier transform, each shifted according to $\boldsymbol{k}_\kappa$ (18). Based on this observation, the Fourier representations of the coil sensitivities may also be referred to as the coils' *k*-space kernels.

Owing to the extent of these kernels, each encoding no longer yields a genuine *k*-space sample but rather a weighted integral of data from a certain *k*-space neighborhood. Therefore the encoding operation can no longer be interpreted as sampling the Fourier transform of $M(\boldsymbol{r})$. In a more general mathematical sense the integral in eqn. (4) represents a scalar product, which may be interpreted as the projection of $M(\boldsymbol{r})$ onto $\mathrm{enc}_{\gamma,\kappa}(\boldsymbol{r})$. As a consequence, image reconstruction can no longer be accomplished by mere Fourier transform but amounts to recovering $M(\boldsymbol{r})$ from a set of more general projections.

The most important aspect of the transition to hybrid encoding functions is that different coils have different sensitivities and hence different *k*-space kernels. This means that, with an array of receiver coils, one can perform multiple different encodings at one time. It is instructive to ask how this is possible in view of the inability to accomplish the same with gradient encoding. A short answer to this question is that the two mechanisms rely on different physics and use different carriers of image information. An attempt of a more detailed answer is sketched in the following.

It is helpful in this context to consider the RF fields that all portions of magnetization jointly generate by their precession. These fields vary in both space and time and hold all image information that can possibly be extracted with a receiver coil. The gradient mechanism encodes the position of a magnetization vector in the frequency and phase of its precession, relying on spin physics as governed by the Bloch equations. The frequency and phase modulation then translates to the electromagnetic fields that the magnetization generates. In other words, gradient encoding stores image information only in the temporal degrees of freedom of the RF fields. This is not surprising given that the concept was once adopted from a spectroscopy method (19).

However, as mentioned above, the relevant RF fields also have spatial degrees of freedom. Every small portion of magnetization generates a characteristic spatial distribution of electric and magnetic RF fields, governed by electrodynamics as described by Maxwell's equations. As a result, the RF fields' spatial degrees of freedom store a significant amount of image information. In conventional MRI with a single coil this information is lost when collapsing the spatially varying fields into a single voltage value. As opposed to that, with multiple receiver coils at different positions at least some of the inherent spatial variation is preserved. In this fashion, the image information encoded in the spatial electrodynamic degrees of freedom is partly recovered.

To summarize this point, gradient encoding recruits only the temporal degrees of freedom of electrodynamics as carriers of image information. Clearly, only one such degree of freedom can be read out at any single point in time. The spatial degrees of freedom of electrodynamics are *per se* carriers of substantial image information in an MRI experiment. Parallel detection is a way of tapping these inherently parallel information channels, yielding data of distinct information content simultaneously.

In principle the electrodynamics offer an infinite number of spatial degrees of freedom. Nevertheless, the amount of image information that can be extracted from them is limited, as has been established in several recent studies (20–22). The main reason for the limitation is that those field components that exhibit the strongest spatial variation decay rapidly with the distance from their source. Therefore the ability to detect them outside the object is greatly reduced.

The difference in nature between the two encoding mechanisms is relevant also in another respect. Owing to the different underlying physics they do not interfere and can hence be freely combined. Note that most contrast mechanisms used in MRI are, like gradient encoding, based on spin physics. As a consequence the additional encoding via the electrodynamic pathway does not perturb the image contrast. Jointly these favorable properties form the basis for the extraordinary versatility

of parallel imaging. It permits virtually any conventional MRI technique to be enhanced without affecting the basic interpretation of the imaging results (15,16).

SAMPLING STRATEGIES

Simultaneous encoding by coil sensitivity can be used to complement gradient encoding and hence to reduce the number of gradient-encoding steps required for one image. It is an important and as yet largely unanswered question how the reduced set of sampling positions in *k*-space can be optimally chosen. With few exceptions (11,23,24), implementations so far have mostly followed the rule of thumb that parallel detection permits reducing the density of *k*-space sampling, while its extent needs to be roughly maintained. This can be understood, at least qualitatively, from Fig. 1, illustrating that the hybrid encoding functions retrieve *k*-space information from the neighborhood of the nominal $\boldsymbol{k}_\kappa$ but hardly across larger distances.

In most MRI techniques the plane-wave vector $\boldsymbol{k}$ is varied in a continuous fashion, following a prescribed *k*-space trajectory. In principle, the sampling density can then be reduced in two ways, by reducing the density of the trajectory as such or by reducing the sampling frequency along the trajectory. However, the latter is of little use because it reduces only the data rate but not the readout duration. Hence, parallel imaging is usually performed with full sampling rate but enhanced distance between adjacent trajectory segments. In common spin-warp techniques this means that the spacing of phase encoding steps is increased, while reducing their number. Similarly, with spiral and radial schemes the sampling density can be reduced by reducing the radial distance of spiral revolutions (9,25,26) or the angular spacing of radii (9,27,28), respectively.

IMAGE RECONSTRUCTION

Continuous formulation

Generally, image reconstruction amounts to recovering $M(\boldsymbol{r})$ from the sampled data $d_{\gamma,\kappa}$, corresponding to inverting eqn. (4). Since the encoding functions no longer form a Fourier basis, this cannot be achieved by mere Fourier transform, requiring more general reconstruction approaches. As in standard Fourier MRI the reconstruction problem faced in parallel MRI is *per se* vastly underdetermined due to finite *k*-space coverage. Therefore image reconstruction generally aims only at estimating $M(\boldsymbol{r})$ at a finite number of positions $\boldsymbol{r}_\rho$, which form the image grid.

Note that the encoding equation (4) is linear in $M(\boldsymbol{r})$. Consequently, all current methods for parallel imaging reconstruction generate the image values (pixels) i_ρ as linear combinations of the raw data:[1]

$$i_\rho = \sum_{\gamma,\kappa} F_{\rho,(\gamma,\kappa)}\, d_{\gamma,\kappa} \qquad (5)$$

where F denotes the net reconstruction matrix. Assembling the data and image values in the vectors $\boldsymbol{d}$, $\boldsymbol{i}$, respectively, eqn. (5) is more conveniently rewritten in matrix notation as

$$\boldsymbol{i} = F\,\boldsymbol{d} \qquad (6)$$

Ideally, each image value i_ρ should exclusively reflect the magnetization at the very position $\boldsymbol{r}_\rho$, which is not possible with finite *k*-space coverage. Instead, each image value will at best reflect signal from a certain volume around $\boldsymbol{r}_\rho$ and exhibit contamination from a greater distance. These imperfections are expressed by the individual pixel's spatial response function (SRF), which in this case reads

$$srf_\rho(\boldsymbol{r}) = \sum_{\gamma,\kappa} F_{\rho,(\gamma,\kappa)}\, enc_{\gamma,\kappa}(\boldsymbol{r}) \qquad (7)$$

Based on the SRF the problem of parallel imaging reconstruction can be viewed as choosing the entries of the reconstruction matrix such that each $srf_\rho(\boldsymbol{r})$ approximates a Dirac peak at $\boldsymbol{r}_\rho$:

$$srf_\rho(\boldsymbol{r}) \rightarrow \delta_\rho(\boldsymbol{r} - \boldsymbol{r}_\rho) \qquad (8)$$

Discrete formulation

One intuitive approach for solving this problem is least-squares approximation (8). In standard Fourier MRI this is straightforward because the plane-wave encoding functions are orthogonal and readily yield discrete Fourier transform (DFT) as the least-squares solution. In parallel imaging the situation is more complicated because the encoding basis is no longer orthogonal. Least-squares reconstruction is still feasible, yet numerically demanding (29). Therefore all of the currently more widespread approaches rely on a mild simplification, which consists in limiting the Dirac approximation to the discrete image grid given by the pixel positions $\boldsymbol{r}_\rho$. Upon discretization the SRFs jointly assume the structure of a matrix given by

$$SRF_{\rho,\rho'} = \sum_{\gamma,\kappa} F_{\rho,(\gamma,\kappa)}\, enc_{\gamma,\kappa}(\boldsymbol{r}_{\rho'}) \qquad (9)$$

[1]Despite the linearity of the encoding equation, nonlinear reconstruction can be prompted by nonlinear constraints or image models (49), which are beyond the scope of this survey. In current parallel imaging root-sum-of-squares combination of single-coil images is sometimes used in a final reconstruction step. In this case the analysis based on eqn. (5) holds only for the single-coil images prior to this nonlinear operation.

The values of the encoding functions on the image grid form the encoding matrix

$$E_{(\gamma,\kappa),\rho} = enc_{\gamma,\kappa}(\boldsymbol{r}_\rho) = s_\gamma(\boldsymbol{r}_\rho)\, e^{j\boldsymbol{k}_\kappa \boldsymbol{r}_\rho} \qquad (10)$$

In this discrete formulation the task of approximating Dirac SRFs reads

$$SRF = FE \rightarrow Id \qquad (11)$$

where Id denotes the $n_i \times n_i$ identity matrix, n_i being the number of pixels to reconstruct. The remaining reconstruction problem is shown schematically in Fig. 2(a). It is significantly simplified by the discretization. As long as the number of coils is at least as large as the degree of k-space undersampling, the encoding matrix will usually have sufficient rank to enable forming the desired identity SRF matrix. Then one exact solution of the approximation task is the Moore–Penrose inverse of E:

$$F = (E^H E)^{-1} E^H, \qquad (12)$$

where the superscript H denotes the complex conjugate transpose. If E has full rank and more rows (i.e. encodings) than columns (i.e. pixels to resolve), there are multiple solutions, meaning that there is more than one way of forming discrete Dirac SRFs from the discrete encoding functions. In other words, some image information was redundantly sampled and can be averaged with arbitrary relative weights. One criterion for choosing these weights is minimizing noise propagation from the raw data into the resulting image values. How the noise superimposes upon averaging depends on the strength and correlation of noise in the input data, which can be described by a noise covariance matrix. Denoting the noise covariance by Ψ, minimal noise and hence maximal SNR for each pixel is obtained with (8)

$$F = (E^H \Psi^{-1} E)^{-1} E^H \Psi^{-1} \qquad (13)$$

Note that, in the limiting case of no encoding redundancy (i.e. E is square), eqn. (13) becomes independent of Ψ and both eqns. (12) and (13) yield $F = E^{-1}$, as one should expect. Another interesting limiting case is full Fourier encoding with multiple coils. In this situation eqn. (13) is equivalent to coil-wise DFT reconstruction and maximum-SNR combination, as described by Roemer *et al.*(17). In the case of full Fourier encoding with a single, homogeneously sensitive coil, finally, both eqns. (12) and (13) yield $F = E^H$, i.e. standard Fourier reconstruction with inverse DFT.

In the general parallel imaging case, evaluating eqns. (12) and (13) is numerically demanding because the encoding matrix is typically very large, e.g. with eight coils, an image matrix of 128×128 and 4-fold Cartesian undersampling, E has $8 \cdot 128^2/4 = 32\,768$ rows and $128^2 = 16\,384$ columns, making straightforward inversion impractical. However, various and quite different ways have been identified to solve the inversion problem efficiently. None of the currently used approaches were derived exactly in the way described here. It is nevertheless instructive to view and compare them using this common framework.

K-SPACE APPROACHES

The encoding matrix, as defined in eqn. (10), is fully populated and often the larger part of its entries are of significant magnitude. This corresponds to the fact that the encoding functions have a large extent in the image domain, as illustrated in Fig. 1. By comparison they are much more compact in k-space, where each has only the extent of its coil kernel. One class of parallel imaging techniques, in particular SMASH (7,12) and GRAPPA (13), capitalize on this relative compactness by addressing the reconstruction problem entirely in k-space. Within the framework described above this transition can be formally implemented by Fourier-transforming eqn. (11) along its spatial dimensions, using DFT:

$$DFT\ F\ E\ DFT^{-1} \rightarrow DFT\ DFT^{-1} \qquad (14)$$

Defining the k-space versions of the encoding and reconstruction matrices,

$$E^{(k)} = E\, DFT^{-1}, \quad F^{(k)} = DFT\, F \qquad (15)$$

the reconstruction task (14) reduces to

$$F^{(k)} E^{(k)} \rightarrow Id \qquad (16)$$

Note that eqn. (15) implies

$$F = DFT^{-1}\, F^{(k)}. \qquad (17)$$

Hence with this approach the overall reconstruction F begins with k-space reconstruction, $F^{(k)}$, followed by inverse DFT of the combined data.

The advantage of the k-space view is illustrated in Fig. 2(b), assuming 2-fold Cartesian undersampling in a schematic one-dimensional imaging situation. The rows of $E^{(k)}$ are the discretized coil kernels, shifted according to $\boldsymbol{k}_\kappa$. $E^{(k)}$ has relatively few large entries, which are grouped around the diagonal in each single-coil block. For two- or three-dimensional imaging the band structure is somewhat more complicated. Irrespectively, the key point is that due to the sparseness of $E^{(k)}$ the desired identity matrix can be approximated with relatively few entries in $F^{(k)}$.

The elementary implementation of this approach is the original SMASH technique, using a single entry of $F^{(k)}$ per row and per coil (7). This corresponds to forming a suitably shifted Dirac function by linear combination of coil kernels, or, in the image-domain view, forming a low-order harmonic (i.e. a plane wave) by linear combination of coil sensitivities. In this fashion, one nearby k-space sample from each coil is retrieved for reconstructing a k-space value of the final image. This is illustrated in the top row of Fig. 2(b), as well as in Fig. 3. Since the blocks of $E^{(k)}$ are only approximately diagonal,

this approach will generally yield only an approximation to the desired identity *k*-space response. One option for improving the fit is constructing suitably modulated functions instead of pure harmonics (30).

Another option is staying in the pure *k*-space picture and involving a larger number of coefficients in $F^{(k)}$. This is done in the GRAPPA technique, which includes data from an extended neighborhood along the

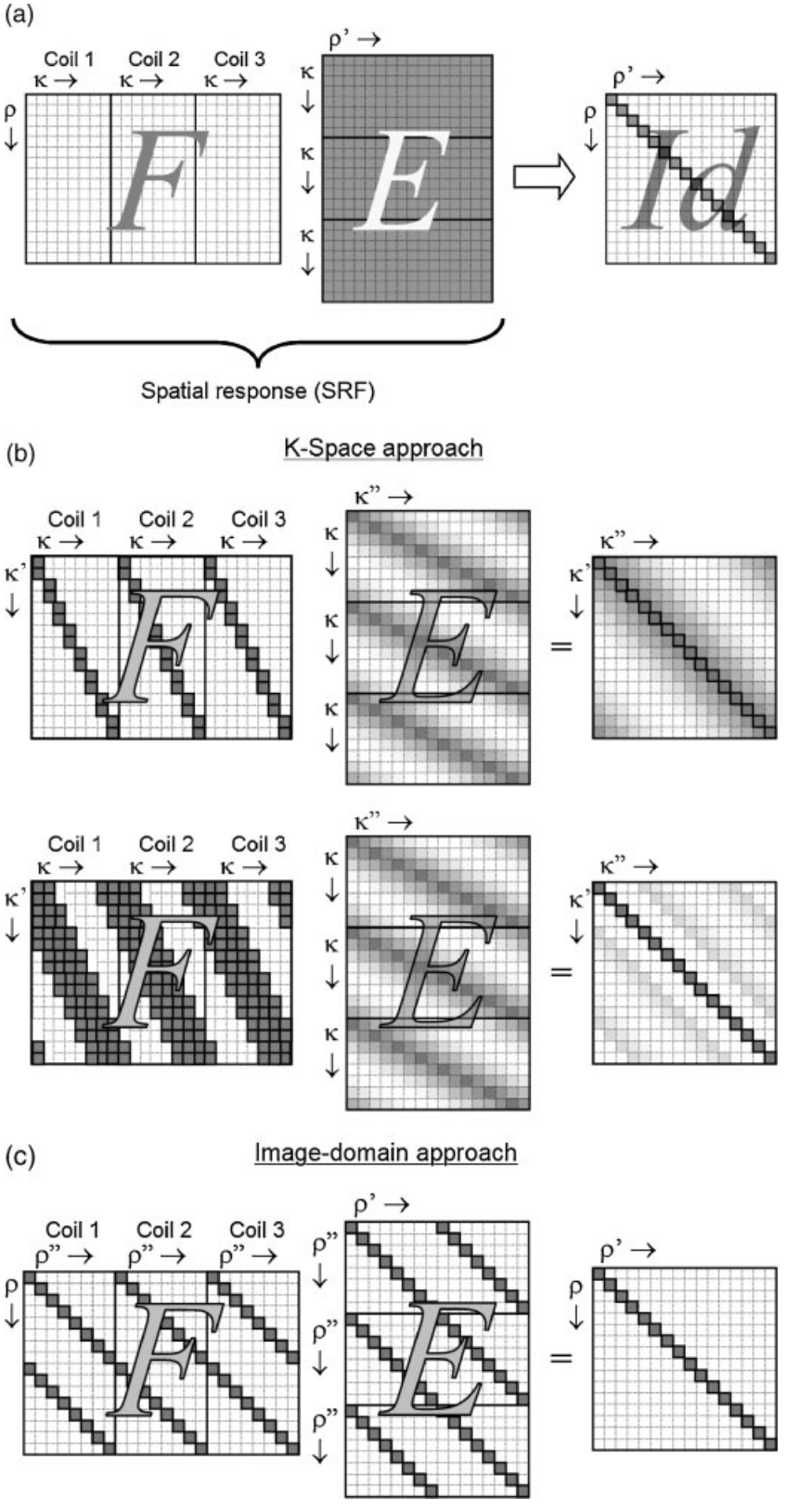

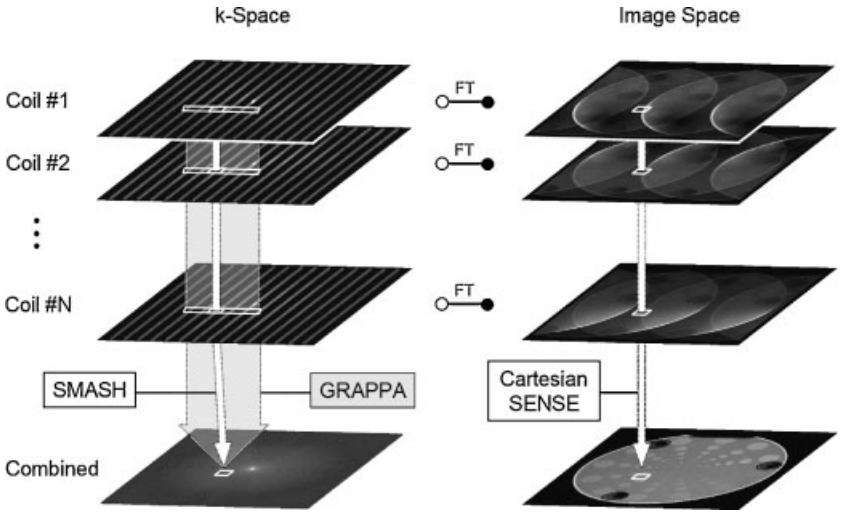

Figure 3. Image reconstruction from Cartesian data. The SMASH and GRAPPA techniques operate in *k*-space. For reconstructing one *k*-space value of the target image, SMASH retrieves one *k*-space sample per coil, while GRAPPA involves neighboring data along the phase encoding direction. Cartesian SENSE operates in the image domain, calculating each pixel from the corresponding set of pixels in the aliased single-coil images

phase-encoding direction (Fig. 3). In this fashion the desired identity response is approximated more closely [Fig. 2(b), bottom row]. In principle all phase-encoding steps can be used. However, satisfactory results can be obtained by including as few as four to eight data samples per coil (13).

A special aspect of GRAPPA is that the coil weights (i.e. the entries of $F^{(k)}$) are not calculated from separately determined coil sensitivities but learned from the undersampled data set. To this end a limited portion of *k*-space is sampled with full density, building upon the concept of Auto-SMASH (31–33). With lattice sampling (34), including Cartesian patterns, the appropriate coil weights are shift-invariant. In this case they need to be learned only once and can be efficiently reused throughout *k*-space.

IMAGE-DOMAIN APPROACHES

The *k*-space picture was obtained by Fourier transform along the spatial dimensions of eqn. (11). Fourier transform can likewise be used for creating an image-domain perspective, namely by transforming E along its *k*-space dimensions:

$$F\,DFT_c\,DFT_c^{-1}\,E \rightarrow Id \qquad (18)$$

where DFT_c represents separate DFT for each individual coil:

$$DFT_c = \begin{pmatrix} DFT & 0 & \cdots & 0 \\ 0 & DFT & \ddots & \vdots \\ \vdots & \ddots & \ddots & 0 \\ 0 & \cdots & 0 & DFT \end{pmatrix}. \qquad (19)$$

Defining the image-domain versions of the encoding and reconstruction matrices,

$$E^{(i)} = DFT_c^{-1}\,E, \quad F^{(i)} = F\,DFT_c \qquad (20)$$

eqn. (18) can be rewritten as the image-domain version of the reconstruction problem:

$$F^{(i)}E^{(i)} \rightarrow Id \qquad (21)$$

Equation (20) implies that

$$F = F^{(i)}\,DFT_c^{-1} \qquad (22)$$

so image-domain reconstruction begins with coil-wise inverse DFT, followed by combining the single-coil data in the image domain.

Figure 2. Schematic of the reconstruction problem in parallel MRI (assuming 2-fold *k*-space undersampling with three coils). (a) The product of the reconstruction matrix F and the encoding matrix E yields the spatial response functions (SRF) of the resulting image values. F must be chosen such that the SRF matrix approaches identity. (b) The *k*-space formulation of the reconstruction problem is obtained by Fourier transform of F, E and Id along their spatial dimensions. In the SMASH method, one entry in F per row and per coil is used, yielding an approximation of the desired identity response (top row). In GRAPPA, a better approximation is accomplished by using more coefficients (bottom row). (c) The image-domain picture is obtained by Fourier transform of F, E along their *k*-space dimensions. With lattice sampling, E assumes a simple form, permitting identity-SRF reconstruction with a single coefficient per row per coil

The image domain picture was first used in the early works of Kelton *et al.*(3) and Ra *et al.*(6) and later became the basis of the Cartesian version of the SENSE technique (8,35). It is schematically illustrated in Fig. 2(c), for the same imaging situation as assumed in Fig. 2(b). Again, the structure of $E^{(i)}$ was considerably simplified by the Fourier transform. Its rows are the discrete SRFs of the pure Fourier imaging, multiplied by the coil sensitivities. Owing to the regularity of Cartesian undersampling, the Fourier SRF is also highly regular, causing equidistant aliasing among disjoint cliques of few pixels (two each in this case). As a result the inversion problem disintegrates into a large number of small, mutually independent inversion problems, each of which amounts to unfolding one clique of aliased pixels. In this situation a single entry per row and per coil is sufficient for implementing an exact inverse $F^{(i)}$, e.g. the Moore–Penrose inverse (eqn 12) or the maximum-SNR inverse (eqn 13).

A special case of image-domain reconstruction occurs when each row of $E^{(i)}$ contains only one significant entry despite incomplete Fourier encoding. This can be the case when the individual coil sensitivities are strongly localized such that each encompasses only one pixel out of each aliasing clique. In this case maximum-SNR reconstruction reduces to matched-filter combination as described by Roemer *et al.*(17), requiring knowledge of $s_\gamma(\boldsymbol{r})$ and the noise covariance Ψ. If this side information is not available, a magnitude image can still be reconstructed by root-sum-of-squares combination, as done in the PILS method (10,36). In doing so it is important to assign each coil's signal to the correct pixel within the respective aliasing clique.

With Cartesian undersampling and, more generally, with any lattice sampling pattern, the image-domain picture permits exact reconstruction with minimal computation. Its efficiency reflects the fact that reconstructing a pixel in the final image involves only one pixel in each single-coil image (Fig. 3). It is important to note though that, by virtue of the initial DFT operation, all raw data are involved in the reconstruction of every pixel in the final image. Hence the equivalent *k*-space reconstruction matrix $F^{(k)}$ would generally be fully populated. It can be determined using eqns. (15) and (22):

$$F^{(k)} = DFT\ F^{(i)}\ DFT_c^{-1} \qquad (23)$$

Likewise, any given *k*-space reconstruction can be transformed into its image-domain equivalent:

$$F^{(i)} = DFT^{-1}\ F^{(k)}\ DFT_c \qquad (24)$$

GENERAL SAMPLING PATTERNS

Both *k*-space and image-domain reconstruction benefit strongly from lattice sampling. In the *k*-space picture, lattice sampling renders the optimal reconstruction coefficients shift-invariant, which essentially reduces their application to a convolution operation. The concept of self-calibration from a densely sampled *k*-space region, as used in GRAPPA, also relies on the shift-invariance of the reconstruction coefficients.

In the image domain, lattice sampling translates into a Fourier SRF that also has lattice structure, corresponding to highly regular aliasing among small, disjoint pixel cliques (34,37). As described above, it is this property that reduces the numerical demands of image domain reconstruction to a minimum.

With general sampling patterns these properties hold no longer or only partly, hence requiring additional considerations and more computation. With certain scanning strategies the benefits of lattice sampling are at least partially available. For instance, spin warp imaging with arbitrary spacing in the phase-encoding direction still exhibits lattice sampling structure in the readout direction. In this case the reconstruction problem can be simplified by transforming it into the image domain at least in the readout dimension. This was proposed in the original work introducing the SPACERIP technique (11). Other patterns such as radial and spiral sampling exhibit approximate lattice structure within limited regions of *k*-space. For these situations the GRAPPA technique has recently been modified to operate with an individual set of reconstruction coefficients in each such region (38–40) (Fig. 4).

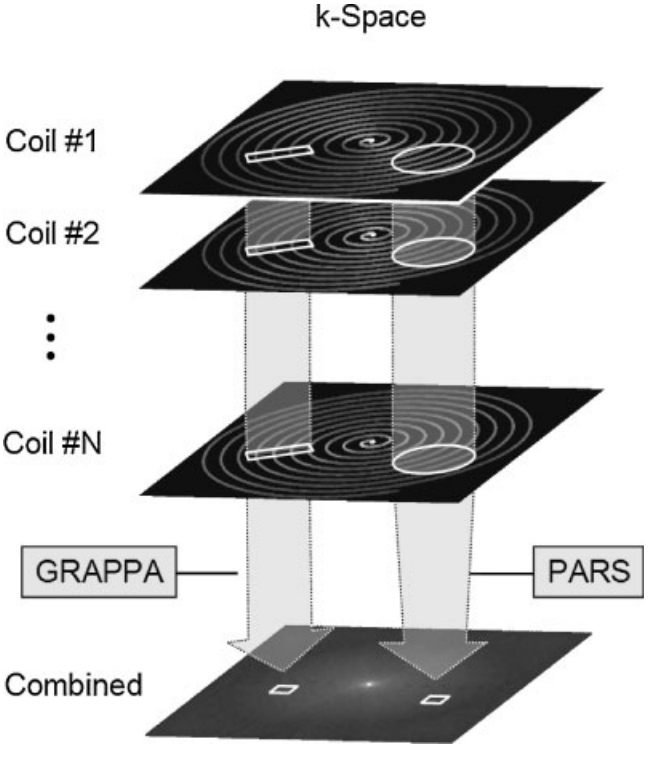

Figure 4. Image reconstruction from non-Cartesian data. With non-Cartesian data the GRAPPA approach can still be used in subregions with regular sampling structure. Another *k*-space approach, PARS, involves all single-coil data within a certain *k*-space radius for constructing a target *k*-space value

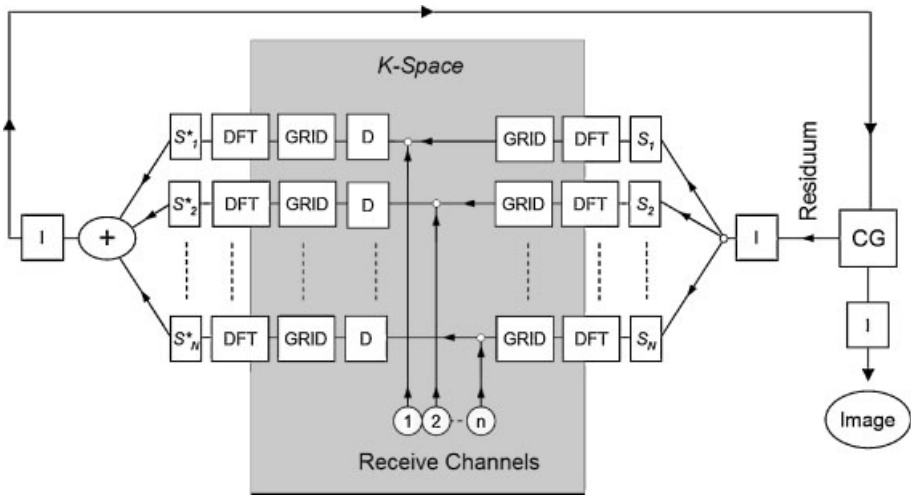

Figure 5. Iterative reconstruction based on the conjugate-gradient (CG) method. In each loop the current residuum image undergoes various operations in the image domain and *k*-space: *I* = correction for inhomogeneous overall sensitivity of the array; $s_\nu^{(*)}$ = multiplication by (complex conjugate of) coil sensitivity; DFT = discrete Fourier transform; GRID = forward and backward regridding; D = sampling density correction

Without relying on lattice properties one can still benefit from the limited *k*-space extent of the coil kernels. The *k*-space-based PARS technique (14,41) does so by restricting the pool of raw data for reconstructing a *k*-space value to a neighborhood of limited radius. In this fashion the single comprehensive inversion problem can be broken down into many smaller, local ones (Fig. 4).

Finally, despite its considerable size, the general inversion problem can also be tackled as a whole. This is currently impractical with direct inversion methods, requiring on the order of N^6 operations for an $N \times N$ image. However, this complexity can be massively reduced by using iterative inversion algorithms. Figure 5 shows a schematic of an iterative approach (9), based on the conjugate gradient (CG) method. To make such an algorithm efficient it is important to perform all matrix operations in an appropriate domain where they are most efficient. For this purpose the algorithm switches back and forth between the image domain and *k*-space. In this fashion, multiplications by coil sensitivity (s_ν) and correction for overall array sensitivity (I) can be performed in the image domain, where they are represented by diagonal matrices. Likewise, sampling density correction (D) is diagonal in *k*-space. Accounting for Fourier encoding is also most efficient in *k*-space, where the corresponding operations (GRID) are almost diagonal. Optionally they can be fully diagonalized by the transition to a *k*-space grid with doubled density (42). However, the savings in computation thus achieved tend to be nearly balanced by greater efforts for the Fourier transforms (43). With or without this additional measure, the aforementioned steps reduce the complexity of each loop of the algorithm from N^4 to $N^2 \log N$, which is the same as that of conventional gridding reconstruction (44). In this fashion, maximum-SNR reconstruction with eqn. (13) can be accomplished in the range of seconds to minutes (9,43), depending on the convergence speed and targeted accuracy.

Switching back and forth between the two domains, the described iterative reconstruction is neither a *k*-space nor an image-domain approach but rather takes advantage of both where appropriate. Nevertheless, the reconstruction matrix thus implemented could again be viewed in either domain. As suggested in Fig. 6, it is generally fully populated in both pictures, retrieving information from all raw data, as well as, equivalently, from all pixels in aliased single-coil images.

NOISE AND SNR

The survey given in this paper has focused on the problem of accurately reconstructing the MR signal component in parallel imaging data. Besides the signal fidelity, the usefulness of the resulting image also depends on its SNR and hence on the noise level in the image. The many ramifications of this issue are beyond the scope of this article but have been studied in many previous works ((8,36,45,46), among others). Here only some key aspects of noise propagation in parallel imaging reconstruction shall be briefly mentioned.

A certain level of stochastic, Gaussian-distributed noise is present in all MR data, arising from thermal agitation of charges throughout the entire experimental setup. The propagation of such noise can be readily formalized. Using any reconstruction matrix F the noise covariance in the resulting image is given by

$$X = F \Psi F^H \qquad (25)$$

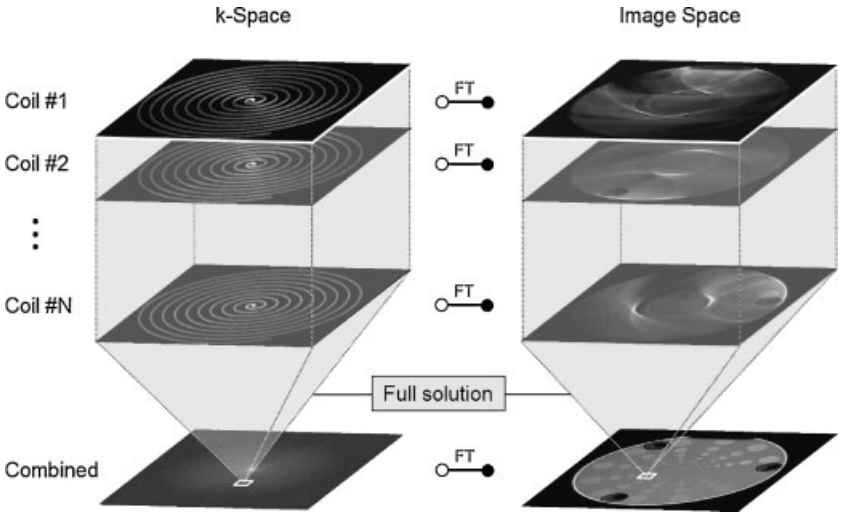

Figure 6. Full solution of the general reconstruction problem. With non-lattice sampling an exact reconstruction will generally involve all raw data in the reconstruction of each target *k*-space value. Likewise, in the image domain view, all pixels in single-coil images contribute to each pixel in the reconstructed image

where Ψ is again the covariance matrix of noise in the input data. The diagonal elements of X are the noise variances of the individual pixels.

Parallel imaging is generally prone to adverse noise behavior because the hybrid encoding functions are not orthogonal. Lack of orthogonality can cause bad conditioning of the inverse problem, which leads to large entries in F and hence to noise enhancement. For the case of lattice sampling and maximum-SNR reconstruction, this phenomenon has been expressed in terms of the so-called geometry factor, which reflects loss in SNR efficiency relative to standard Fourier imaging (8). Critically large geometry factors tend to occur primarily with high acceleration factors, corresponding to strong Fourier undersampling.

Excessive noise amplification can be avoided by regularization (29,30,47,48). In doing so, one trades accuracy of the matrix inversion for stability of the solution. In the context of image reconstruction this means that the quality of the spatial response is compromised in favor of the image's SNR. Regularization is also a generic way of addressing noise propagation into parts of *k*-space that were not sampled at all, like for example the corners of *k*-space in spiral acquisition. Alternatively, such noise can be removed with a straightforward *k*-space filter (9).

OUTLOOK

For several years, image reconstruction has been one of the key problems in parallel imaging and has thus prompted major research efforts. As a result, the basic reconstruction problem is now fairly well understood and a number of feasible solutions have been identified. In particular, for most of the numerous applications of parallel MRI, image reconstruction is now routinely accomplished with satisfactory speed and image quality. However, important challenges remain, of which only three prominent ones shall be listed here.

One is the increasing need to manage and process very large amounts of data. This development is driven by the continuous increase in the number of coil elements, as well as by growing demand for temporally resolved and three-dimensional imaging. Hence the efficiency of image reconstruction will remain a key issue.

Further progress is also required in the broad context of coil calibration. As the number of coil array elements increases, the individual coil size decreases, enhancing the spatial frequency content of the coil sensitivity functions. This trend enhances the demands on coil calibration as well as issues related to geometric inconsistency over time of non-rigid coil configurations. The need for larger amounts of reference data favors calibration by a separate scan, while the latter problem will be easier to handle with embedded calibration. So the choice between separate and embedded approaches will remain interesting and important.

Finally, most of the existing reconstruction methods for parallel imaging address the encoding effect of coil sensitivity as the sole deviation from pure Fourier encoding. However, in imaging practice one faces various additional imperfections, including B_0 inhomogeneity, tissue motion and eddy current effects. Working these into the reconstruction formalism and identifying efficient solutions will be a critical and challenging step in exploring the full potential of the parallel paradigm.

REFERENCES

1. Carlson JW. An algorithm for NMR imaging reconstruction based on multiple RF receiver coils. *J. Magn. Reson*. 1987; **74**(2): 376–380.
2. Hutchinson M, Raff U. Fast MRI data acquisition using multiple detectors. *Magn. Reson. Med*. 1988; **6**(1): 87–91.
3. Kelton JR, Magin RL, Wright SM. An algorithm for rapid image acquisition using multiple receiver coils, in *Proc. Society for Magn. Reson. Med., 8th Annual Meeting*, Amsterdam, 1989, p. 1172.
4. Kwiat D, Einav S, Navon G. A decoupled coil detector array for fast image acquisition in magnetic-resonance-imaging. *Med. Phys*. 1991; **18**(2): 251–265.
5. Carlson JW, Minemura T. Imaging time reduction through multiple receiver coil data acquisition and image reconstruciton. *Magn. Reson. Med*. 1993; **29**(5): 681–687.
6. Ra JB, Rim CY. Fast imaging using subencoding data sets from multiple detectors. *Magn. Reson. Med*. 1993; **30**(1): 142–145.
7. Sodickson DK, Manning WJ. Simultaneous acquisition of spatial harmonics (SMASH): fast imaging with radiofrequency coil arrays. *Magn. Reson. Med*. 1997; **38**(4): 591–603.
8. Pruessmann KP, Weiger M, Scheidegger MB, Boesiger P. SENSE: sensitivity encoding for fast MRI. *Magn. Reson. Med*. 1999; **42**(5): 952–962.
9. Pruessmann KP, Weiger M, Bornert P, Boesiger P. Advances in sensitivity encoding with arbitrary *k*-space trajectories. *Magn. Reson. Med*. 2001; **46**(4): 638–651.
10. Griswold MA, Jakob PM, Nittka M, Goldfarb JW, Haase A. Partially parallel imaging with localized sensitivities (PILS). *Magn. Reson. Med*. 2000; **44**(4): 602–609.
11. Kyriakos WE, Panych LP, Kacher DF, Westin CF, Bao SM, Mulkern RV, Jolesz FA. Sensitivity profiles from an array of coils for encoding and reconstruction in parallel (SPACE RIP). *Magn. Reson. Med*. 2000; **44**(2): 301–308.
12. Bydder M, Larkman DJ, Hajnal JV. Generalized SMASH imaging. *Magn. Reson. Med*. 2002; **47**(1): 160–170.
13. Griswold MA, Jakob PM, Heidemann RM, Nittka M, Jellus V, Wang JM, Kiefer B, Haase A. Generalized autocalibrating partially parallel acquisitions (GRAPPA). *Magn. Reson. Med*. 2002; **47**(6): 1202–1210.
14. Yeh EN, McKenzie CA, Ohliger MA, Sodickson DK. Parallel magnetic resonance imaging with adaptive radius in *k*-space (PARS): constrained image reconstruction using *k*-space locality in radiofrequency coil encoded data. *Magn. Reson. Med*. 2005; **53**(6): 1383–1392.
15. van den Brink JS, Watanabe Y, Kuhl CK, Chung T, Muthupillai R, Van Cauteren M, Yamada K, Dymarkowski S, Bogaert J, Maki JH, Matos C, Casselman JW, Hoogeveen RM. Implications of SENSE MR in routine clinical practice. *Eur. J. Radiol*. 2003; **46**(1): 3–27.
16. Heidemann RM, Ozsarlak O, Parizel PM, Michiels J, Kiefer B, Jellus V, Muller M, Breuer F, Blaimer M, Griswold MA, Jakob PM. A brief review of parallel magnetic resonance imaging. *Eur. Radiol*. 2003; **13**(10): 2323–2337.
17. Roemer PB, Edelstein WA, Hayes CE, Souza SP, Mueller OM. The NMR phased-array. *Magn. Reson. Med*. 1990; **16**(2): 192–225.
18. Wang Y. Description of parallel imaging in MRI using multiple coils. *Magn. Reson. Med*. 2000; **44**(3): 495–499.
19. Kumar A, Welti D, Ernst RR. NMR Fourier zeugmatography. *J. Magn. Reson*. 1975; **18**: 69–85.
20. Ohliger MA, Grant AK, Sodickson DK. Ultimate intrinsic signal-to-noise ratio for parallel MRI: electromagnetic field considerations. *Magn. Reson. Med*. 2003; **50**(5): 1018–1030.
21. Wiesinger F, Boesiger P, Pruessmann KP. Electrodynamics and ultimate SNR in parallel MR imaging. *Magn. Reson. Med*. 2004; **52**(2): 376–390.
22. Wiesinger F, van de Moortele P-F, Adriany G, de Zanche N, Ugurbil K, Pruessmann KP. Parallel imaging performance as a function of field strength—an experimental investigation using electrodynamic scaling. *Magn. Reson. Med*. 2004; **52**(5): 953–964.
23. Jacob M, Xu D, Liang Z-P. Optimal selection of phase encodings in parallel MR imaging, in *Proc. Second International Workshop on Parallel MRI*, Zurich, 2004; 55. Available at: www.mr.ethz.ch/parallelmri04.
24. Fattahi S, Rutt BK. Pushing the speed limit in SENSE using novel sampling strategies, in *Proc. Second International Workshop on Parallel MRI*, Zurich, 2004; 57. Available at: www.mr.ethz.ch/parallelmri04.
25. Weiger M, Pruessmann KP, Osterbauer R, Bornert P, Boesiger P, Jezzard P. Sensitivity-encoded single-shot spiral imaging for reduced susceptibility artifacts in BOLD fMRI. *Magn. Reson. Med*. 2002; **48**(5): 860–866.
26. Qian Y, Zhang Z, Stenger VA, Wang Y. Self-calibrated spiral SENSE. *Magn. Reson. Med*. 2004; **52**(3): 688–692.
27. Bammer R, Vigen KK, Pruessmann KP, Markl M, Moseley ME. Self-calibrating radial generalized SENSE, in *Proc. International Society for Magn. Reson. Med., 12th Meeting*, Kyoto, 2004; 2414.
28. Arunachalam A, Du J, Mistretta CA, Block WF. Parallel imaging techniques for contrast-enhanced mr angiography using 3D non-cartesian trajectories, in *Proc. Second International Workshop on Parallel MRI*, Zurich, 2004; 56. Available at: www.mr.ethz.ch/parallelmri04.
29. Tsao J, Sanchez J, Boesiger P, Pruessmann KP. Minimum-norm reconstruction for optimal spatial response in high-resolution SENSE imaging, in *Proc. International Society for Magn. Reson. Med., 11th Meeting*, Toronto, 2003; 14.
30. Sodickson DK. Tailored SMASH image reconstructions for robust *in vivo* parallel MR imaging. *Magn. Reson. Med*. 2000; **44**(2): 243–251.
31. Jakob PM, Griswold MA, Edelman RR, Sodickson DK. AUTO-SMASH: a self-calibrating technique for SMASH imaging. *Magn. Reson. Mater. Phys. Biol. Med*. 1998; **7**(1): 42–54.
32. Heidemann RM, Griswold MA, Haase A, Jakob PM. VD-AUTO-SMASH imaging. *Magn. Reson. Med*. 2001; **45**(6): 1066–1074.
33. Park J, Zhang Q, Jellus V, Simonetti O, Li D. Artifact and noise suppression in GRAPPA imaging using improved *k*-space coil calibration and variable density sampling. *Magn. Reson. Med*. 2005; **53**(1): 186–193.
34. Willis NP, Bresler Y. Lattice-theoretic analysis of time-sequential sampling of spatiotemporal signals—Part II: large space-bandwidth product asymptotics. *IEEE Trans. Inform. Theory* 1997; **13**: 208–220.
35. Weiger M, Pruessmann KP, Boesiger P. 2D SENSE for faster 3D MRI. *Magn. Reson. Mater. Phys. Biol. Med*. 2002; **14**(1): 10–19.
36. Madore B, Pelc NJ. SMASH and SENSE: experimental and numerical comparisons. *Magn. Reson. Med*. 2001; **45**(6): 1103–1111.
37. Tsao J, Boesiger P, Pruessmann KP. *k-t* BLAST and *k-t* SENSE: dynamic MRI with high frame rate exploiting spatiotemporal correlations. *Magn. Reson. Med*. 2003; **50**(5): 1031–1042.
38. Griswold MA, Heidemann RM, Jakob PM. Direct parallel imaging reconstruction of radially sampled data using GRAPPA with relative shifts, in *Proc. 11th Annual Meeting of ISMRM*, Toronto, 2003; 2349.
39. Heberlein KA, Kadah Y, Hu X. Segmented spiral parallel imaging using GRAPPA, in *Proc. 12th Annual Meeting of ISMRM*, Kyoto, 2004; 328.
40. Heidemann RM, Griswold MA, Kruger G, Kannengiesser S, Kiefer B, Jakob PM. Fast parallel image reconstruction for spiral trajectories, in *Proc. Second International Workshop on Parallel MRI*, Zurich, 2004; 27. Available at: www.mr.ethz.ch/parallelmri04.
41. Yeh EN, Stuber M, McKenzie CA, Ohliger MA, Grant AK, Willig JD, Sodickson DK. Self-calibrated spiral parallel imaging, in *Proc. 10th Annual Meeting ISMRM*, Honolulu, HI, 2002; 2390.
42. Wajer FTAW, Pruessmann KP. Major speedup of reconstruction for sensitivity encoding with arbitrary trajectories, in *Proc. International Society for Magn. Reson. Med., 9th Meeting*, Glasgow, 2001; 767.
43. Eggers H, Boernert P, Boesiger P. Comparison of gridding- and convolution-based iterative reconstruction algorithms for sensitivity-encoded non-cartesian acquisition, in *Proc. International Society for Magn. Reson. Med., 10th Meeting*, Honolulu, HI, 2002; p. 743.
44. Jackson JI, Meyer CH, Nishimura DG, Macovski A. Selection of a convolution function for Fourier inversion using gridding. *IEEE Trans. Med. Imag*. 1991; **MI-10**: 473–478.

45. Sodickson DK, Griswold MA, Jakob PM, Edelman RR, Manning WJ. Signal-to-noise ratio and signal-to-noise efficiency in SMASH imaging. *Magn. Reson. Med*. 1999; **41**(5): 1009–1022.
46. Weiger M, Boesiger P, Hilfiker PR, Weishaupt D, Pruessmann KP. Sensitivity encoding as a means of enhancing the SNR efficiency in steady-state MRI. *Magn. Reson. Med*. 2005; **53**(1): 177–185.
47. Sanchez-Gonzalez J, Tsao J, Dydak U, Desco M, Boesiger P, Pruessmann KP. Minimum-norm reconstruction for sensitivity-encoded magnetic resonance spectroscopic imaging. *Magn. Reson. Med*. 2006; **55**(2): 287–295.
48. Lin FH, Kwong KK, Belliveau JW, Wald LL. Parallel imaging reconstruction using automatic regularization. *Magn. Reson. Med*. 2004; **51**(3): 559–567.
49. Lustig M, Lee JH, Donoho DL, Pauly JM. Faster imaging with randomly perturbed, undersampled spirals and $|L|_1$ reconstruction, in *Proc. International Society for Magn. Reson. Med., 13th Meeting*, Miami, FL, 2005; 685.

